Hindawi
Mathematical Problems in Engineering
Volume 2019, Article ID 1245213, 14 pages
https://doi.org/10.1155/2019/1245213

Research Article

Potential Launch Opportunities for a SmallSat Mission around the Moon Injected during a Lunar Flyby En Route to Mars

Yongjun Song,[1] **Young-Joo Song**,[2] **Seongwhan Lee**,[1] **Kap-Sung Kim**,[1] **and Ho Jin**[1]

[1]*School of Space Research, Kyung Hee University, Yongin 17104, Republic of Korea*
[2]*Lunar Exploration Program Office, Korea Aerospace Research Institute, Daejeon 34133, Republic of Korea*

Correspondence should be addressed to Young-Joo Song; dear.yjsong@gmail.com

Received 2 May 2019; Revised 18 August 2019; Accepted 31 August 2019; Published 24 September 2019

Academic Editor: Florin Stoican

In this work, the concept of a multipurpose mission that can explore both the Moon and Mars with a single launch is proposed, and potential launch opportunities are analyzed to establish an early-phase trajectory concept. The proposed mission applies the concept of a piggyback ride to a small-sized lunar probe, i.e., the daughtership, of the main Mars orbiter, i.e., the mothership. For the trajectory design, the Earth-Moon-Mars gravity assist (EMMGA) trajectory is adopted for the mothership to reach Mars, and the daughtership is assumed to be released from the mothership during lunar flyby. To investigate the early-phase feasibility of the proposed mission, the launch windows have been analyzed and the associated delta-Vs have been directly compared with the solutions obtained for typical Earth-Mars direct (EMD) transfer options. The identified launch windows (in the years 2031 and 2045) could be the strongest candidates for the proposed conceptual mission. Under the current assumptions, up to approximately 15% (in 2031) and 9% (in 2045), more dry mass is expected to be delivered to Mars by appropriately selecting one of the currently available launch vehicles, regardless of whether the EMMGA transfer option is used. For missions around the Moon using a SmallSat in 2031, the feasibility of a lunar orbiter case and an impactor case is briefly analyzed based on the delta-Vs required to divert the SmallSat from the mothership. Although the current work is performed under numerous assumptions for a simplified problem, the narrowed candidate launch window from the current work represents a good starting point for more detailed trajectory design optimization and analysis to realize the proposed conceptual mission.

1. Introduction

For many scientific reasons, interest in interplanetary exploration for scientific discovery purposes is currently rising. The National Aeronautics and Space Administration (NASA) announced its goal of a human exploration mission to Mars and is first focusing on the return of humans to the surface of the Moon. As a part of this plan, NASA will construct a lunar orbital platform called the Gateway, which is a modular space station located in near rectilinear halo orbit (NRHO) between the Earth and the Moon [1]. The Gateway will serve as the gateway for lunar landing and further deep space missions [2]. By utilizing the Gateway, NASA plans to land the first female astronaut on the Moon by 2024 and aims to establish a sustainable human presence on the Moon by 2028 [3]. As the paradigm for planetary exploration has shifted, many fascinating studies have been conducted on orbital stabilities and low-energy transfers [4–12]. Further details on the relevant literature are left for the readers to discover, as there exists a significant amount of research.

Also of interest when designing interplanetary missions is the reduction of the overall mission cost while reliably achieving the original scientific and technological mission objectives. In general, the total mission costs for interplanetary missions can be reduced by using a number of approaches, such as by minimizing the required overall delta-Vs to accomplish the mission, by designing the mission trajectory to target multiple planets within a single launch, or by designing missions that can be performed with a small-sized spacecraft.

Most of the launch windows for interplanetary missions are usually designed to minimize the required delta-Vs, and the flyby technique is occasionally applied to reduce the

overall mission cost. A flyby, which is a gravity-assisted flight, utilizes the gravity of a celestial body to change the spacecraft's direction or speed, thus allowing the spacecraft to gain or lose energy without any additional fuel consumption. The flyby technique can be adapted to design transfer trajectories between other planets or central body bounding trajectories directed toward another planet by using the natural moon [13]. This flyby technique has enabled interplanetary missions requiring high inclination changes relative to the ecliptic plane with limited performance of the launch vehicle [14]. Moreover, by applying the flyby technique, not only can delta-V budgets be minimized, but the opportunity to visit additional planets in a single launch can be gained. This concept is called a multipurpose space mission because it allows for the exploration of several targets in a single mission [15].

In addition to minimizing overall mission costs by finding the best launch windows, either for direct or flyby missions, the overall mission costs and riskiness will be greatly reduced if interplanetary missions are performed with a small-sized spacecraft. With current technological improvements, diverse scientific data can be collected at an extremely low cost if a small-sized spacecraft is used for solar system exploration missions [16]. Indeed, the NASA Innovative Advanced Concepts Program (NIAC) has planned small, low-cost missions beyond the low Earth orbit using CubeSats [17]. Additionally, the first Mars exploration CubeSat, MarCO (Mars Cube One), was launched with a Mars lander called InSight on May 2018, and it sent an image from Mars [18]. Moreover, conceptual CubeSat missions for other solar system objects, such as Io [19] and Deep Space Gateway (DSG) [20], have been proposed recently.

One of the most important concerns during the early design stage of a Mars mission is finding a solution that can reduce the overall mission cost while maximizing the scientific and technological gains. One of the solutions could be building a mothership that can carry a small satellite as an onboard payload to achieve a lunar flyby en route to Mars, which certainly will provide additional opportunities to explore the Moon with a single launch. During the mothership's lunar flyby phase, a small satellite could be released to orbit the Moon and perform its own mission to achieve its designated scientific goals. After the release of a small satellite, the mothership continues its journey to Mars to accomplish its main mission objectives. This concept also benefits the system reliability of a small satellite's bus compared with an interplanetary mission planned with only the small satellite itself because a small satellite's bus can be effectively protected from planetary hazards, such as thermal and radiation hazards, during the journey to the Moon [21, 22].

Many authors have revealed the usefulness of utilizing a lunar flyby when designing an interplanetary mission. Farquhar and Dunham [23] reported that double lunar swingby maneuvers increase the C3 value from –0.5 to $4.5\,\mathrm{km}^2/\mathrm{s}^2$ and suggested that double and triple lunar flybys could potentially offer trips to the planets. Hanson et al. [24] analyzed the potential of an Earth-Mars trajectory by using single and multiple lunar flybys to improve the available payload gain. Kawaguchi et al. [25] designed a real Earth-Mars trajectory for the Japanese Mars exploration spacecraft, NOZOMI, using a similar double lunar flyby method. Hernandez and Barbee [26] considered using a single lunar flyby for the Near-Earth Asteroids (NEA) mission, and their main objective when adapting lunar flybys to explore NEA was to reduce the total required delta-Vs during the overall mission sequences. They concluded that a lunar flyby is more effective than a direct transfer for exploring NEA. All these studies concluded that lunar flyby methods allow a spacecraft to depart Earth at a lower energy than that needed to escape and then proceed to planetary encounters. Although many studies apply the concept of lunar flyby to design Earth escape trajectories, most of these studies applied multiple lunar gravity assists to maximize delta-V savings. Similar work was conducted by Hanson et al. [24] in the 1990s. In Ref. [24], many lunar flyby options were considered, but multiple lunar gravity assists were focused on rather than a single flyby to reduce the delta-V budget. The application of multiple lunar gravity will lead to very complex mission operations, which have already been discussed as a disadvantage of the multiple gravity assist [24]. Furthermore, feasibility studies on Mars transfer trajectory design with a single lunar flyby have rarely been performed. Most importantly, no recent work has proposed and analyzed possible Mars mission launch opportunities using single lunar flyby for the upcoming decades. Providing such future launch opportunities is very important in further realizing the proposed conceptual mission. Therefore, the current work investigates suitable launch opportunities of a Mars mission by using only a single lunar flyby to support the emerging SmallSat piggyback ride planetary mission concept. Utilization of single lunar flyby will ultimately ease the mission operation and minimize overall mission riskiness, which will be a driving factor of mission success.

The main objective of the current study is to perform an early-phase feasibility study on a proposed conceptual multipurpose mission. The realization of such a mission first requires trajectory design studies that estimate the overall mission delta-V budgets. The current study investigates launch opportunities for an Earth-Mars mission utilizing a flyby of the Moon, and it includes an estimation of the required overall delta-V budgets. For the first step, to roughly estimate overall mission delta-V budgets, the current work employed a simplified methodology, the patched conic method with simplified equations of motion, to determine potential launch years. The obtained delta-V budgets are compared with typical delta-V values obtained using Earth-Mars direct transfer options. The mothership's mass budget characteristics are also roughly investigated using currently available data on heavy launch vehicle performance. Additionally, the mass budgets for a SmallSat mission around the Moon deployed from a mothership were estimated. Although the current work utilized well-known methodologies to derive results, it is expected that the current work can make the following contributions: First, both mission designers and supervisors who are interested in SmallSat application to interplanetary missions can gain insight while establishing similar mission concepts. Second,

the current work can serve as a reference for further work related to launch opportunities in the near future. Finally, based on the results of the current work, detailed trajectory design solutions can be advanced by implementing an optimization algorithm with N-body equations of motion and with more realistic mission constraint parameters. The remainder of this manuscript is organized as follows: Detailed simulation procedures, including equations of motion based on the patched conic method, are described in Section 2. The numerical implications and assumptions for setting up the simulation are provided in Section 3. Detailed simulation results and an associated discussion are presented in Section 4. The conclusions are discussed in Section 5.

2. Models and Methods

This section describes the models and methods used to design an Earth-Moon-Mars gravity assist (EMMGA) trajectory and determine the orbit of a lunar SmallSat. In this paper, we use a single lunar flyby method similar to that described by Hernandez and Barbee [26] to calculate the EMMGA trajectory. The EMMGA trajectory is designed using the patched conic method. This method uses a series of conic sections patched together to form a trajectory bounded by the central body, which primarily affects the motion of the spacecraft. For a detailed discussion of this method, readers can refer to the papers by Barbee et al. [27] and Hernandez and Barbee [26]. In this method, the EMMGA trajectory is divided into three phases: Earth-centered, Sun-centered and Mars-centered. In the Earth-centered phase, the mothership releases the SmallSat during the lunar flyby phase, and the released SmallSat is then captured by the Moon with an onboard thruster. After the flyby, the mothership is ejected to an Earth-escape hyperbola that leads to Mars after a Sun-centered interplanetary cruise phase. During the Mars-centered phase, the mothership arrives at the Mars sphere of influence and enters the Mars parking orbit. To design the Earth's sphere of influence (SOI) escape trajectory, it is assumed that the mothership uses only a single, unpowered lunar gravity assist. However, multiple lunar gravity assist techniques can be applied for this phase rather than a single flyby to reduce the delta-V budget. Indeed, reducing overall delta-V cost by utilizing multiple gravity assist is another important factor that should be considered during the early mission design phase. However, as discussed, the current work is focused on investigating suitable launch opportunities under a single lunar flyby. Lastly, the delta-Vs in the current work are assumed to be impulsive burns during each phase.

2.1. Lunar Flyby Trajectory Generation En Route to Mars

2.1.1. Earth-Centered Phase (Stage 1). The first step in designing the trajectory consists of targeting a lunar flyby in the Earth-centered phase. In this stage, the trajectory of the mothership is designed using four-body equations of motion. Four-body equations of motion can be replaced with two-body equations of motion in this Earth-centered phase for preliminary trajectory design purposes. However, the current work adopted four-body equations of motion to increase the maturity of the trajectory solutions obtained through this work, and these equations can be used as a basis of further work regarding the detailed optimization of high-fidelity dynamic models. The equations of motion of the mothership with Earth as the primary central body and the Moon and Sun as perturbing bodies in the Earth-centered Earth mean equator and equinox of epoch J2000 (EEME2000) coordinate system are expressed in [28, 29]:

$$\dot{\mathbf{r}}_{\mathrm{E-SC}} = \mathbf{v}_{\mathrm{E-SC}}, \tag{1a}$$

$$\dot{\mathbf{v}}_{\mathrm{E-SC}} = -\frac{\mu_{\mathrm{E}}}{\left|\dot{\mathbf{r}}_{\mathrm{E-SC}}\right|^3}\mathbf{r}_{\mathrm{E-SC}} + \mathbf{g}_{\mathrm{E-L}} + \mathbf{g}_{\mathrm{E-S}}, \tag{1b}$$

where $\mathbf{r}_{\mathrm{E-SC}}$, $\mathbf{v}_{\mathrm{E-SC}}$, and $\dot{\mathbf{r}}_{\mathrm{E-SC}}$ denote the position, velocity, and acceleration vectors of the mothership with respect to the Earth, respectively, μ_{E} is the gravitational constant of the Earth, and $\mathbf{g}_{\mathrm{E-L}}$ and $\mathbf{g}_{\mathrm{E-S}}$ are the perturbing gravitational forces of the Moon and Sun with Battin's q function, respectively, which can be expressed as follows [28, 30]:

$$\mathbf{g}_{\mathrm{E-L}} = -\frac{\mu_L}{\left|\mathbf{r}_{\mathrm{L-SC}}\right|^3}\left[\mathbf{r}_{\mathrm{E-SC}} + F(q_{\mathrm{L}})\mathbf{r}_{\mathrm{E-L}}\right], \tag{2a}$$

$$\mathbf{g}_{\mathrm{E-S}} = -\frac{\mu_{\mathrm{s}}}{\left|\mathbf{r}_{\mathrm{S-SC}}\right|^3}\left[\mathbf{r}_{\mathrm{E-SC}} + F(q_{\mathrm{s}})\mathbf{r}_{\mathrm{E-S}}\right], \tag{2b}$$

where μ_{L} and μ_{S} are the gravitational constants of the Moon and Sun, respectively, and $\mathbf{r}_{\mathrm{L-SC}}$ and $\mathbf{r}_{\mathrm{S-SC}}$ are the position vectors from the Moon and Sun to the mothership, respectively. The q functions for the Moon, $F(q_{\mathrm{L}})$, and the Sun, $F(q_{\mathrm{S}})$, are expressed as follows:

$$F(q_{\mathrm{L}}) = q_{\mathrm{L}}\left[\frac{3 + 3q_{\mathrm{L}} + q_{\mathrm{L}}^2}{1 + \left(\sqrt{1 + q_{\mathrm{L}}}\right)^3}\right], \tag{3a}$$

$$q_{\mathrm{L}} = \frac{\left|\mathbf{r}_{\mathrm{E-SC}}\right|^2 - 2\mathbf{r}_{\mathrm{E-SC}} \cdot \mathbf{r}_{\mathrm{L-SC}}}{\left|\mathbf{r}_{\mathrm{L-SC}}\right|^2}, \tag{3b}$$

$$F(q_{\mathrm{S}}) = q_{\mathrm{S}}\left[\frac{3 + 3q_{\mathrm{S}} + q_{\mathrm{S}}^2}{1 + \left(\sqrt{1 + q_{\mathrm{S}}}\right)^3}\right], \tag{3c}$$

$$q_{\mathrm{S}} = \frac{\left|\mathbf{r}_{\mathrm{E-SC}}\right|^2 - 2\mathbf{r}_{\mathrm{E-SC}} \cdot \mathbf{r}_{\mathrm{S-SC}}}{\left|\mathbf{r}_{\mathrm{S-SC}}\right|^2}. \tag{3d}$$

The initial conditions of equations (1a) and (1b) can be defined with the initial position ($\mathbf{r}_0$) and velocity vectors ($\mathbf{v}_0$) of the mothership as follows:

$$\mathbf{r}_0 = \mathbf{r}_{\mathrm{E-SC}}^{\mathrm{p}}, \tag{4a}$$

$$\mathbf{v}_0 = \mathbf{v}_{\mathrm{E-SC}}^{\mathrm{p}} + \Delta\mathbf{V}_{\mathrm{Dep}}, \tag{4b}$$

where $\mathbf{r}_{\mathrm{E-SC}}^{\mathrm{p}}$ and $\mathbf{v}_{\mathrm{E-SC}}^{\mathrm{p}}$ are the position and velocity vectors of the mothership on the initial Earth parking orbit, respectively, and $\Delta\mathbf{V}_{\mathrm{Dep}}$ is defined as the delta-V vector required to transfer the mothership to the Moon under four-body dynamics.

To derive $\mathbf{r}^{\mathrm{p}}_{\mathrm{E-SC}}$, $\mathbf{v}^{\mathrm{p}}_{\mathrm{E-SC}}$, and $\Delta\mathbf{V}_{\mathrm{Dep}}$, the current work used Ramanan's pseudostate method [31] and slight corrections were made to the obtained results for application in four-body dynamics. Ramanan's method is a very powerful and effective method based on two-body dynamics, and it solves Lambert problem iteratively to generate initial conditions of transfer trajectories for moon missions. Of course, the best way to obtain $\mathbf{r}^{\mathrm{p}}_{\mathrm{E-SC}}$, $\mathbf{v}^{\mathrm{p}}_{\mathrm{E-SC}}$, and $\Delta\mathbf{V}_{\mathrm{Dep}}$ is to apply an optimization algorithm under a high-fidelity dynamic model. However, the current work used Ramanan's pseudostate method to focus on the preliminary analysis. To use Ramanan's pseudostate method, the user must first define the following parameters: the translunar injection (TLI) maneuver time (t_{TLI}), the Earth-Moon transfer time ($t_{\mathrm{tof\_E-M}}$), and initial Earth parking orbit elements (i.e., semimajor axis (a_{p}), eccentricity (e_{p}), inclination (i_{p}), and argument of the perigee (ω_{p})). In addition, the user should select a preferred TLI maneuver location. Usually, there are two possible maneuver execution locations on the initial parking orbit for a given t_{TLI}: one during the ascending motion of the parking orbit and the other during the descending motion. Once these parameters are given, the Ramanan's pseudostate method can be used to calculate the remaining parking orbit elements (i.e., the right ascension of the ascending node (Ω_{p}), the true anomaly (υ_{p}), and the minimum TLI maneuver vector ($\Delta\mathbf{v}_{\mathrm{TLI\_2body}}$). For additional details on Ramanan's pseudostate method, refer to Ref. [31].

After applying Ramanan's pseudostate method, the state vectors of the mothership in the Earth parking orbit ($\mathbf{r}^{\mathrm{p}}_{\mathrm{E-SC}}$ and $\mathbf{v}^{\mathrm{p}}_{\mathrm{E-SC}}$) and $\Delta\mathbf{v}_{\mathrm{TLI\_2body}}$ are obtained, where $\Delta\mathbf{v}_{\mathrm{TLI\_2body}}$ is the minimum TLI maneuver vector derived under two-body dynamics. As the current work used four-body equations of motion during the Earth-centered phase, $\Delta\mathbf{V}_{\mathrm{Dep}}$, as shown in equations (4a) and (4b), cannot be directly replaced with $\Delta\mathbf{v}_{\mathrm{TLI\_2body}}$. Therefore, $\Delta\mathbf{V}_{\mathrm{Dep}}$ is obtained in relation to $\Delta\mathbf{v}_{\mathrm{TLI\_2body}}$, as follows:

$$\Delta\mathbf{V}_{\mathrm{Dep}} = \left|\Delta\mathbf{v}_{\mathrm{TLI\_2body}}\right| + \Delta\mathbf{V}_{\mathrm{add}}, \tag{5a}$$

$$\Delta\mathbf{V}_{\mathrm{Dep}} = \Delta\mathbf{V}_{\mathrm{Dep}} \times \frac{\Delta\mathbf{v}_{\mathrm{TLI\_2body}}}{\left|\Delta\mathbf{v}_{\mathrm{TLI\_2body}}\right|}. \tag{5b}$$

As shown in equations (5a) and (5b), a small velocity magnitude correction, $\Delta\mathbf{V}_{\mathrm{add}}$, is made to the magnitude of $\Delta\mathbf{v}_{\mathrm{TLI\_2body}}$ while maintaining the same direction as that of $\Delta\mathbf{v}_{\mathrm{TLI\_2body}}$. The direction of $\Delta\mathbf{V}_{\mathrm{Dep}}$ will not actually be exactly the same as that of $\Delta\mathbf{v}_{\mathrm{TLI\_2body}}$, but the current work accepted this assumption, as the delta-V magnitude change rate plays a more significant role in the resultant trajectory solutions than the direction change rates unless the estimated delta-V directions are completely insufficient. The current work obtained proper ranges of $\Delta\mathbf{V}_{\mathrm{add}}$ based on trial and error by investigating the behaviors of the resultant trajectory. Within the given ranges of $\Delta\mathbf{V}_{\mathrm{add}}$, $\Delta\mathbf{V}_{\mathrm{add}}$ that minimizes $\Delta\mathbf{V}_{\mathrm{Dep}}$ while satisfying the lunar flyby condition is selected as a candidate $\Delta\mathbf{V}_{\mathrm{add}}$.

After the initial state vectors required to perform a lunar flyby ($\mathbf{r}_0$ and $\mathbf{v}_0$) are determined, the trajectory of the Earth-Moon system is propagated with stopping conditions for the mothership when it reaches the Earth's SOI after a single lunar flyby over a time span of $t_{\mathrm{tof\_SOI}}$. The radial distance of the Earth's SOI, R_{SOI}, is given as 924,500 km. When the trajectory reaches the Earth's SOI after a lunar flyby, the mothership's state vectors ($\mathbf{r}_{\mathrm{SOI}}$ and $\mathbf{v}_{\mathrm{SOI}}$) are located on the boundary of the Earth's SOI at t_{SOI}, which can be simply calculated as $t_{\mathrm{SOI}} = t_{\mathrm{TLI}} + t_{\mathrm{tof\_SOI}}$. During propagation, two different constraints are used to ensure that the generated trajectory is a lunar flyby. The first constraint is given as $h > 0$ km, where h is the altitude of the mothership from the surface of the Moon. If h is less than 0 km during the simulation, then the mothership will impact the lunar surface. The second condition is a constraint, $t_{\mathrm{tof\_SOI}}$. The maximum of $t_{\mathrm{tof\_SOI}}$ is given as 20 days during the simulation because the typical mothership's flight time in the Earth's SOI is approximately 10 days when a single lunar flyby is applied. If the mothership cannot reach the Earth's SOI until a $t_{\mathrm{tof\_SOI}}$ of 20 days, then we consider that the mothership is unable to escape from the Earth's SOI after flyby. If the trajectory does not satisfy one or both of these constraints during propagation, then we assume that the EMMGA trajectory is impossible to be generated. Herein, additional constraints should be considered to ensure a practical lunar flyby for real-flight operation. For instance, "face-on" geometry during lunar flyby should be guaranteed for the purpose of Earth communication, and lower limits on flyby altitude and velocity should be set, as these conditions are strongly related not only to the mothership but also to SmallSat's bus design, especially the fuel budget. Nevertheless, the current work omits details of these additional constraints, as they can be derived only after further establishment of detailed mission concepts and goals.

2.1.2. Sun-Centered Phase (Stage 2). When the mothership escapes from the Earth's SOI, the gravity of the Sun becomes the dominant force. In this phase, the motion of the mothership is primarily affected by the Sun, and the perturbations of other planetary bodies are neglected. To describe the motion of the mothership in the Sun-centered phase, the state vectors of the mothership are transformed into a heliocentric ecliptic coordinate system, thus producing the following equations:

$$\mathbf{r}^{\mathrm{S}}_{\mathrm{SOI}} = \mathbf{M}\left(t_{\mathrm{SOI}}\right)\left(\mathbf{r}_{\mathrm{SOI}} + \mathbf{r}^{\mathrm{S}}_{\mathrm{E}}\right), \tag{6a}$$

$$\mathbf{v}^{\mathrm{S}}_{\mathrm{SOI}} = \mathbf{M}\left(t_{\mathrm{SOI}}\right)\left(\mathbf{v}_{\mathrm{SOI}} + \mathbf{v}^{\mathrm{S}}_{\mathrm{E}}\right), \tag{6b}$$

where $\mathbf{r}_{\mathrm{SOI}}$ and $\mathbf{v}_{\mathrm{SOI}}$ are the state vectors of the mothership with respect to the Earth, as previously discussed, $\mathbf{r}^{\mathrm{S}}_{\mathrm{SOI}}$ and $\mathbf{v}^{\mathrm{S}}_{\mathrm{SOI}}$ are the position and velocity vectors of the mothership with respect to the Sun-centered frame, respectively, and $\mathbf{r}^{\mathrm{S}}_{\mathrm{E}}$ and $\mathbf{v}^{\mathrm{S}}_{\mathrm{E}}$ are the Earth's state vectors with respect to the Sun, which are calculated from the precise ephemerides. The matrix $\mathbf{M}\left(t_{\mathrm{SOI}}\right)$ is the rotation matrix that converts the state vector from equatorial coordinates to ecliptic coordinates at t_{SOI} [32–34].

After converting the states, the trajectory from the Earth's SOI to Mars' SOI can be simply calculated via the Lambert problem in the heliocentric coordinate system. To solve the Lambert problem, the previously calculated $\mathbf{r}^{S}_{SOI}$ and t_{SOI} as well as the Mars arrival time (t_{Arr}) and the Sun-centered position of Mars ($\mathbf{r}^{S}_{M}$) at t_{Arr} are required. By solving the Lambert problem, the required velocity at the Earth's SOI ($\mathbf{v}^{S}_{Dep\_SOI}$) and at Mars' arrival ($\mathbf{v}^{S}_{Arr\_M}$) can be easily calculated. Once the Lambert solution is found, the required delta-V for leaving the Earth's SOI, $\Delta\mathbf{V}_{SOI}$, can be simply calculated as follows:

$$\Delta\mathbf{V}_{SOI} = \left|\mathbf{v}^{S}_{Dep\_SOI} - \mathbf{v}^{S}_{SOI}\right|. \tag{7}$$

The method adapted to compute $\Delta\mathbf{V}_{SOI}$ in the current study is mainly used to adapt the patched conic method to focus on the preliminary analysis. Notably, computing delta-V at the SOI may not be efficient from an energetic point of view, requiring further improvement through optimization using N-body dynamics. For example, instead of imparting the delta-V at the moment of SOI crossing, the following options can be considered in upcoming work. First, a powered lunar flyby that imparts the delta-V at the moment just after periapsis passage of the Moon can be considered. Imparting the delta-V just after periapsis seems to be a reasonable option under the current mission concepts with regard to deployment of the SmallSat during the lunar flyby of the mothership. Performing a maneuver before the lunar flyby may be another option, but this approach could result in a higher delta-V requirement to release the SmallSat due to the increase in the periapsis velocity and certainly requires further study. Finally, the utilization of a powered Earth flyby can be considered. For this option, the mothership can fly back to Earth after completion of a single lunar flyby and impart the delta-V to depart to Mars at the moment of periapsis passage of Earth, which still satisfies the utilization of a single lunar flyby to avoid mission complexities.

2.1.3. Mars-Centered Phase (Stage 3). When the mothership arrives at Mars' SOI, the Mars arrival hyperbolic excess velocity with respect to Mars (V_{∞_M}) is calculated as follows:

$$V_{\infty\_M} = \left|\mathbf{v}^{S}_{Arr\_M} - \mathbf{v}^{S}_{M}\right|, \tag{8}$$

where $\mathbf{v}^{S}_{M}$ is Mars' velocity with respect to the Sun at t_{Arr}, which is calculated directly from the ephemerides, and $\mathbf{v}^{S}_{Arr\_M}$ was previously calculated in Section 2.1.2.

If the mothership targets a circular Mars mission orbit, then the required delta-V from the hyperbolic entry orbit into a target circular orbit ($\Delta\mathbf{V}_{Arr}$) can be simply calculated as follows:

$$\Delta\mathbf{V}_{Arr} = \sqrt{\frac{2\mu_M}{a_{p\_M}} + V^2_{\infty\_M}} - \sqrt{\frac{\mu_M}{a_{p\_M}}}, \tag{9}$$

where a_{p_M} is the semimajor axis of the Mars mission orbit, and μ_M is the gravitational constant of Mars. Using equations (5a), (7), and (9), the total delta-V required for the EMMGA trajectory ($\Delta\mathbf{V}_{Total}$) is calculated as in equation (10). The overall conceptual diagram of the mission segment through stage 1–3 and the delta-V maneuver points is schematically shown in Figure 1.

$$\Delta\mathbf{V}_{Total} = \Delta\mathbf{V}_{Dep} + \Delta\mathbf{V}_{SOI} + \Delta\mathbf{V}_{Arr}. \tag{10}$$

2.2. Released SmallSat Trajectory Generation. The equations of motion of the SmallSat released from the mothership during lunar flyby are described with two-body motion as follows:

$$\ddot{\mathbf{r}}_{L-SC} = -\frac{\mu_L}{\left|\mathbf{r}_{L-SC}\right|^3}\mathbf{r}_{L-SC}. \tag{11}$$

In equation (11), $\ddot{\mathbf{r}}_{L-SC}$ and $\mathbf{r}_{L-SC}$ represent the acceleration and position vectors of the SmallSat in the Moon-Centered Moon mean equator and International Astronomical Union (IAU) vector of the epoch J2000 (MMME2000) coordinate system, respectively. Note that the SmallSat is assumed to be released from the mothership at the moment of the mothership's perilune passage (t_p) during flyby. The value of t_p can easily be computed during propagation of the mothership's trajectory under the condition of a flight path angle of 0 degrees.

To evaluate equation (11), the initial state of the SmallSat ($\mathbf{r}_{0L}$, $\mathbf{v}_{0L}$) at t_p can be expressed as follows:

$$\mathbf{r}_{0L} = \mathbf{r}_{p\_m}, \tag{12a}$$

$$\mathbf{v}_{0L} = \mathbf{v}_{p\_m} + \Delta\mathbf{V}_{rel}, \tag{12b}$$

where $\mathbf{r}_{p\_m}$ and $\mathbf{v}_{p\_m}$ are the position and velocity vectors of the mothership at the perilune, respectively, and $\Delta\mathbf{V}_{rel}$ is the delta-V vector required to divert the SmallSat from the mothership. To determine the required total delta-V to perform a SmallSat mission around the Moon ($\Delta\mathbf{V}_{MOI}$), the Hohmann transfer method is used to simplify the given problem; therefore, the direction of the applied delta-V to divert the SmallSat into the mission orbit around the Moon is always opposite the direction of the mothership's velocity. If the SmallSat is an orbiter, a burn ($\Delta\mathbf{V}_{sec}$) other than $\Delta\mathbf{V}_{rel}$ is necessary to circularize the SmallSat's orbit to a target altitude. For this case, $\Delta\mathbf{V}_{MOI}$ can be $\Delta\mathbf{V}_{MOI} = \Delta\mathbf{V}_{rel} + \Delta\mathbf{V}_{sec}$, where $\Delta\mathbf{V}_{sec}$ is the magnitude of the second burn directly obtained by solving the Hohmann transfer problem. However, if the final mission of a SmallSat is an impactor mission, then $\Delta\mathbf{V}_{MOI}$ will have the same magnitude as $\Delta\mathbf{V}_{rel}$, which can be calculated with the target altitude condition of 0 km while solving the Hohmann transfer problem. Setting a 0-km target altitude while solving the Hohmann transfer problem may result in a very shallow impact angle for an impactor, and the resultant delta-Vs may differ from the delta-Vs derived from the current study if a larger impact angle is necessary. However, the current study accepted this assumption to roughly estimate relevant delta-Vs. If the goal of the impactor mission is refined, then the required impact angle condition will certainly be another constraint to consider for more in-depth trajectory design and analysis.

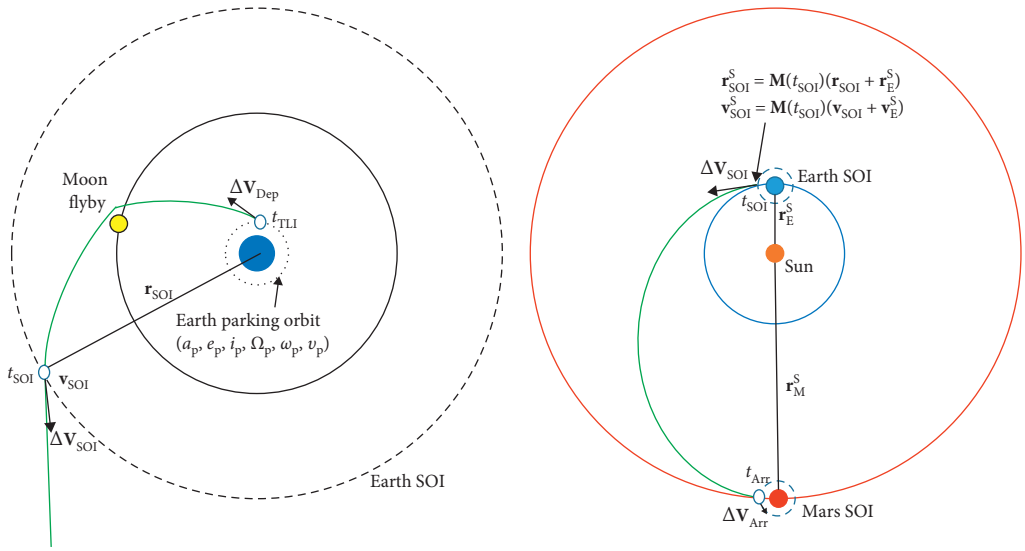

FIGURE 1: EMMGA transfer option schematics. The left side represents the 1st stage transfer trajectory inside of the Earth's SOI, and the right side represents the 2nd and 3rd stage transfer trajectories in the Sun-centered system (not to scale).

2.3. Mass Budget Estimation. From the obtained delta-Vs, the propellant and dry mass of the mothership and the SmallSat can be estimated. In the EMMGA trajectory, two burns ($\Delta \mathbf{V}_{\mathrm{SOI}}$ and $\Delta \mathbf{V}_{\mathrm{Arr}}$) will be executed by the mothership based on our design concept. Therefore, the required propellant and dry mass of the mothership ($m_{\mathrm{p\_m}}$ and $m_{\mathrm{dry\_m}}$) can be easily calculated with the initial mass of the mothership (m_{0_m}), and the specific impulse of the mothership ($I_{\mathrm{sp\_m}}$) is as follows:

$$m_{\mathrm{p\_m}} = m_{0\_\mathrm{m}}\left(1 - \exp\left(\frac{(-\Delta \mathbf{V}_{\mathrm{SOI}} + \Delta \mathbf{V}_{\mathrm{Arr}})}{\mathbf{g}_0 I_{\mathrm{sp\_m}}}\right)\right), \tag{13a}$$

$$m_{\mathrm{dry\_m}} = m_{0\_\mathrm{m}} - m_{\mathrm{p\_m}}, \tag{13b}$$

where $\mathbf{g}_0$ is the gravitational acceleration of Earth.

For the SmallSat, the onboard propulsion system of the SmallSat itself should be used to generate $\Delta \mathbf{V}_{\mathrm{MOI}}$ to orbit or impact the Moon. The required propellant mass of the SmallSat ($m_{\mathrm{p\_s}}$) during lunar capture can be calculated as in equation (13a) with the values of $\Delta \mathbf{V}_{\mathrm{MOI}}$, m_{0_s}, and $I_{\mathrm{sp\_s}}$, where m_{0_s} is the overall initial mass of the SmallSat and $I_{\mathrm{sp\_s}}$ is the specific impulse of the SmallSat's onboard thruster.

3. Simulation Setup

During the simulation, the launch period of the mothership is assumed to be between the years 2026 and 2045. To calculate the precise position, velocity vectors, and physical parameters of the celestial bodies, Jet Propulsion Laboratory (JPL) DE405 ephemerides [32] is used to obtain the gravitational constant, equatorial radius, etc. The hours, minutes, and seconds of t_{TLI} and t_{Arr} for the given dates are assumed as 00 : 00 : 00 in the Universal Coordinate Time (UTC) timescale and converted to the Barycentric Dynamical Time (TDB) timescale to adapt DE405. To perform a simulation, the initial earth departure date, namely, t_{TLI}, is given from Oct. 2026 to Dec. 2045. This time span covers the same analysis duration as that in the work of Burke et al. [35], which analyzed launch opportunities of the EMD transfer option. After the initial t_{TLI} of each year is selected, the corresponding t_{Arr} is calculated as t_{TLI} + 365 days. Additionally, to search for the best departure and arrival dates, the search bounds for t_{TLI} are given by initial t_{TLI} ± 60 days and by ±180 days for the initial t_{Arr}, which leads to a total time of flight (TOF) from Earth to Mars ranging from 125 to 605 days. The t_{SOI} and perilune altitude for the flyby were calculated during the process of patching the problem and were directly used to simulate the current problem.

For numerical integration, the DOPRI8 integrator is used [36, 37], which is based on the 7th to 8th order Runge–Kutta–Fehlberg method with an adaptation of the error control technique from Press et al. [38] with a truncation error tolerance of $\varepsilon = 1 \times 10^{-12}$. For the initial parking orbit conditions during the Earth departure phase, namely, to perform the TLI maneuver, the circular orbit is assumed to have a 300-km altitude with an inclination of 80.0 degrees. The remaining orbital elements Ω_{p} and υ_{p} are properly selected during the simulation, as mentioned in Section 2.1.1. $\Delta \mathbf{V}_{\mathrm{add}}$ is given in the range from −2.0 to 2.0 m/s and increased with 1 m/s steps which were selected based on trial and error during the simulation to satisfy given flyby conditions of the current work. If the search range of $\Delta \mathbf{V}_{\mathrm{add}}$ is smaller than −2.0 m/s, then most of the discovered trajectories are similar to the trajectories obtained with a $\Delta \mathbf{V}_{\mathrm{add}}$ of −2.0 m/s. When $\Delta \mathbf{V}_{\mathrm{add}}$ is larger than 2.0 m/s, the mothership will crash into the Moon or simply return to the vicinity of Earth. The transfer flight time from Earth to the Moon, $t_{\mathrm{tof\_E-M}}$, is varied within the range from 4.0 to 6.0 days with 0.1 day searching steps. When the search range of $t_{\mathrm{tof\_E-M}}$ is extended, no remarkable changes in the simulation results are discovered. For example, when $t_{\mathrm{tof\_E-M}}$ is set to less than

4 days, meaningful delta-V changes throughout the mission are not discovered, and if $t_{\text{tof\_E–M}}$ is set to less than 3 days, then the constraints discussed in Section 2 ($h > 0$, TOF in the Earth SOI < 20 days), which are quite critical for finding a feasible EMMGA transfer option, are not guaranteed. All the parameters selected based on trial and error, as in the current study, must be given as constraints or free parameters. Additionally, with proper control variables nested within the optimal problem with complex dynamics, to improve the efficiency of imparting the delta-V before Earth SOI escape, the overall mission delta-V can be further minimized and more detailed trajectory design trade-off studies can be performed. Finally, the mission orbit of the mothership after arriving on Mars is assumed to be circular with an altitude of 100 km.

4. Results and Analysis

4.1. EMMGA Trajectory Characteristics

4.1.1. Launch Opportunities. To investigate the feasibility of the proposed conceptual mission, the launch opportunities of a mothership that utilizes the EMMGA transfer option should first be analyzed. Indeed, the total delta-V budget between the EMMGA and EMD transfer options should be compared because typical Mars missions utilize the Hohmann-shaped EMD transfer option due to its simplicity and optimality. In Table 1, the major trajectory design parameters for the period from 2026 to 2045 are compared between the EMMGA and EMD transfer options, including the Earth departure date, the Mars arrival date, the delta-Vs at each phase ($\Delta\mathbf{V}_{\text{Dep}}$, $\Delta\mathbf{V}_{\text{SOI}}$, $\Delta\mathbf{V}_{\text{Arr}}$ and $\Delta\mathbf{V}_{\text{Total}}$), the C3 energy, and the transfer type of the EMD trajectory. Note that every value for the EMD transfer options has been directly obtained and regenerated from the work of Burke et al. [35]. Burke et al. [35] showed the best launch windows of the EMD transfer option with four types of EMD trajectory solutions: Type I-A, Type I-B, Type II-A, and Type II-B. Nominally, Type I and Type II trajectories have heliocentric travel angles that are less than and greater than 180 degrees, respectively. In addition, because the orbits of Earth and Mars are neither exactly circular nor coplanar, one launch opportunity may require less departure energy (categorized as Type I-A and Type II-A) or have a lower V_{∞_M} (categorized as Type I-B and Type II-B) than another opportunity. While adapting launch opportunities from the work of Burke et al. [35] for comparison, launch windows exceeding a C3 of Earth departure of 12 km^2/s^2 are neglected to consider the limits of launcher performance. For this reason, the transfer data for 2037 and 2039 are not presented in Table 1.

As expected, the total delta-V magnitude required to accomplish the proposed mission, namely, utilization of the EMMGA transfer options, generally must be greater than that required for the EMD option, regardless of EMD transfer types. Specifically, a delta-V of approximately 7.148–8.006 km/s is required if the EMMGA transfer options is used, and a delta-V of approximately 5.678–7.493 km/s is necessary if the EMD option is adopted. Notably, Table 1 shows that the yearly total delta-V difference between the EMMGA and EMD transfer options varies greatly, even if the Earth departure and Mars arrival timeframes are similar, except for some years within 1- or 2-month differences. For example, if the Mars mission is scheduled for 2026, then the EMMGA transfer option would require approximately 1.44 km/s more delta-V than the EMD transfer. However, if a similar mission is scheduled for 2031, then approximately 0.5 km/s more delta-V can provide another opportunity to visit the Moon and perform another meaningful science mission.

These phenomena appear to be caused by differences in the launch and arrival geometries, including the dates, between the EMMGA and EMD transfer options. The launch and arrival geometry differences will certainly change the orbital energy of the derived mission orbit and the total delta-V. Typically, $\Delta\mathbf{V}_{\text{Dep}}$, which is the delta-V required for a spacecraft to reach target planets (to Mars for the EMD option and to the Moon for the EMMGA option), is within the range from 3.571–3.689 km/s for the EMD transfer options and from 3.101–3.116 km/s for the EMMGA transfer options, showing that the EMD cases require greater departure delta-Vs than the EMMGA cases. This result again confirms that a stronger upper stage of the launch vehicle should be supported for a spacecraft headed to Mars than for those headed to the Moon. However, if the EMMGA transfer option is selected, the Earth departure C3 is approximately –2 km^2/s^2 and increases to approximately 1.1–1.3 km^2/s^2 after lunar flyby, which is far lower than the typical C3 magnitude, which is approximately 8-9 km^2/s^2 for the EMD option. Regarding onboard propulsion delta-V generation, approximately 0.972–2.323 km/s more delta-V should be generated regardless of the mission timeframe difference. This change is primarily due to the additional delta-V requirement, $\Delta\mathbf{V}_{\text{SOI}}$, for the EMMGA cases, which is approximately 1.846–2.324 km/s to insert the mothership into the trans-Mars trajectory.

However, because of different overall TOFs between the EMMGA and EMD transfer cases as well as the mothership's final approach conditions for Mars, the value of V_{∞_M} for the EMMGA transfer option was almost equal or slightly less than that for the EMD transfer option. As shown in Table 1, the $\Delta\mathbf{V}_{\text{Arr}}$ directly calculated using the V_{∞_M} of the EMMGA case is slightly less than that of the EMD case, except for the years 2028 and 2043. For the mission period of 2031, the difference in $\Delta\mathbf{V}_{\text{Arr}}$ between the EMMGA and EMD cases was approximately 1.03 km/s, which ultimately reduced the total delta-V requirement difference between the EMMGA and EMD options to less than approximately 0.5 km/s. As shown in Table 1, the Earth departure C3 value of the year 2045 is considerably larger (more than 10 km^2/s^2) than that of other years. Recalling that there are launch opportunities with a lower departure energy (Type A) or a lower V_{∞_M} (Type B), Table 2 compares the delta-V characteristics of the EMD and EMMGA transfer options with inclusion of both Types A and B for the year 2045. In terms of $\Delta\mathbf{V}_{\text{Total}}$, Type II-B is clearly a better option than Type II-A for EMD transfers, as the $\Delta\mathbf{V}_{\text{Total}}$ of Type II-A substantially increases due to the increase in $\Delta\mathbf{V}_{\text{Arr}}$, namely, V_{∞_M}. At this point, a Mars

Table 1: Comparison of the major trajectory design parameters between the EMD and EMMGA transfer options for the period from 2026 to 2045.

Transfer option	Earth departure date (month, day, year)	Mars arrival date (month, day, year)	$\Delta\mathbf{V}_{\mathrm{Dep}}$ (km/s)	$\Delta\mathbf{V}_{\mathrm{SOI}}$ (km/s)	$\Delta\mathbf{V}_{\mathrm{Arr}}$ (km/s)	$\Delta\mathbf{V}_{\mathrm{SOI}} + \Delta\mathbf{V}_{\mathrm{Arr}}$ (km/s)	C3 ($\mathrm{km}^2/\mathrm{s}^2$)	$\Delta\mathbf{V}_{\mathrm{Total}}$ (km/s)	Transfer type
EMD	Nov. 06, 2026	Sep. 8, 2027	3.633	N/A	2.075	2.075	9.646	5.708	Type II-B
EMMGA	Oct. 25, 2026	Sep. 10, 2027	3.101	1.974	2.073	4.047	N/A	7.148	N/A
EMD	Nov. 20, 2028	Sep. 18, 2029	3.618	N/A	2.270	2.270	9.315	5.888	Type II-B
EMMGA	Nov. 29, 2028	Oct. 14, 2029	3.108	2.066	2.397	4.463	N/A	7.571	N/A
EMD	Feb. 23, 2031	Jan. 09, 2032	3.571	N/A	3.922	3.922	8.237	7.493	Type II-A
EMMGA	Jan. 08, 2031	Nov. 09, 2031	3.112	2.004	2.890	4.894	N/A	8.006	N/A
EMD	Apr. 20, 2033	Nov. 06, 2033	3.616	N/A	2.455	2.455	9.266	6.071	Type I-B
EMMGA	Apr. 10, 2033	Oct. 30, 2033	3.115	1.846	2.446	4.292	N/A	7.407	N/A
EMD	Apr. 21, 2035	Nov. 03, 2035	3.657	N/A	2.134	2.134	10.19	5.791	Type I-A
EMMGA	Jun. 18, 2035	Jan. 13, 2036	3.116	2.035	2.109	4.144	N/A	7.260	N/A
EMD	Oct. 21, 2041	Sep. 04, 2042	3.641	N/A	2.037	2.037	9.819	5.678	Type II-B
EMMGA	Oct. 09, 2041	Aug. 31, 2042	3.104	2.081	2.034	4.115	N/A	7.220	N/A
EMD	Nov. 15, 2043	Sep. 16, 2044	3.603	N/A	2.183	2.183	8.969	5.786	Type II-A
EMMGA	Oct. 19, 2043	Sep. 04, 2044	3.102	2.291	2.212	4.503	N/A	7.605	N/A
EMD	Dec. 03, 2045	Sep. 21, 2046	3.689	N/A	2.425	2.425	10.84	6.114	Type II-B
EMMGA	Nov. 25, 2045	Sep. 25, 2046	3.102	2.324	2.424	4.748	N/A	7.850	N/A

Table 2: Comparison of the EMD and EMMGA trajectory design parameters for the year 2045.

Transfer option	Earth departure date (month, day, year)	Mars arrival date (month. day, year)	$\Delta\mathbf{V}_{\mathrm{Dep}}$ (km/s)	$\Delta\mathbf{V}_{\mathrm{SOI}}$ (km/s)	$\Delta\mathbf{V}_{\mathrm{Arr}}$ (km/s)	$\Delta\mathbf{V}_{\mathrm{SOI}} + \Delta\mathbf{V}_{\mathrm{Arr}}$ (km/s)	C3 ($\mathrm{km}^2/\mathrm{s}^2$)	V_{∞_M} (km/s)	$\Delta\mathbf{V}_{\mathrm{Total}}$ (km/s)	Transfer type
EMD	Dec. 03, 2045	Sep. 21, 2046	3.689	N/A	2.425	2.425	10.84	3.256	6.114	Type II-B
	Jan. 22, 2046	Dec. 18, 2046	3.589	N/A	3.621	5.119	8.587	5.119	7.210	Type II-A
EMMGA	Nov. 25, 2045	Sep. 25, 2046	3.102	2.324	2.424	4.748	N/A	3.255	7.850	N/A

mission can be expected to be carried out most efficiently with an Earth departure C3 of Type II-A and a V_{∞_M} of Type II-B for the year 2045. In this case, one of the candidate launch options that can be considered is EMMGA transfer. Although the EMMGA option requires significantly more delta-Vs than the Type II-B EMD option, selecting the EMMGA option for a 2045 mission may be another very attractive option in terms of launch capabilities and the maximum return of scientific data from a single launch. In fact, the difference in total delta-Vs required between the EMMGA option and Type II-A of the EMD option for this year is only approximately 0.6 km/s, which is slightly greater than that for the year 2031. This phenomenon can again be explained by differences in launch and arrival geometries, including the dates, between the EMMGA and EMD transfer options. If the EMMGA transfer option is selected for the year 2045, as shown in Table 2, then the Earth departure date and arrival date are much closer, with 8 days for departure and 4 days for arrival, to those of Type II-B than to those of Type II-A, which can ultimately reduce the amount of $\Delta\mathbf{V}_{\mathrm{Arr}}$.

Importantly, the current results are derived from a simplified model with several assumptions that must be resolved in more detail. In particular, the total delta-V difference between the EMMGA and EMD options is expected to be further minimized compared to the current findings by applying a more efficient energetic strategy to impart delta-Vs before escaping the Earth's SOI using an implementing optimization algorithm. Consequently, the proposed mission can ultimately reach Mars with an additional opportunity to explore the Moon. The discovery of such a launch window that can perform the proposed mission, even with a similar Earth departure and Mars arrival timeframe, can benefit a wide range of routine work required to realize this mission. Because of the simplicity of the proposed mission, the adoption of a single lunar flyby will certainly reduce the trajectory designers' time and effort required to establish the trajectory concept during the early stage and perform the relevant feasibility analysis. Simultaneously, real-time operation efforts can be minimized to reduce the overall mission risks, which are mostly caused by human factors. Most significantly, the possibility of performing the proposed mission based on the technical readiness of the currently available launch vehicle's performance has been confirmed, and the details of the mass budget estimations will be discussed in the following subsection.

4.1.2. Spacecraft Mass Budget Estimation. This subsection analyzes and compares the expected spacecraft's mass budget characteristics between the EMD and EMMGA transfer options based on the delta-Vs obtained in the previous section. To estimate the mass budget of the spacecraft, the performances of three different currently

available heavy launch vehicles are directly adapted as example cases. In Table 3, the representative payload delivery capabilities to the Moon and Mars are shown for Ariane 5, Proton M, and Atlas V. To compare the spacecraft mass budgets between the EMD and EMMGA transfer options, the payload capabilities for targeting Mars (EMD case) and the Moon (EMMGA case) shown in Table 3 are used. Notably, however, the mass budgets derived in the current section are all rough estimates and may differ for different launch constraints and conditions, including the finalized values of the mission-dependent overall delta-Vs. The payload delivery capabilities shown in Table 3 are derived under the assumption that launchers have the best performance and certain aspects of injection C3 and escape declination [39]. According to the work of Biesbroek [39], the payload delivery capabilities of the launchers shown in Table 3 are all derived under the conditions of $10\,\mathrm{km}^2/\mathrm{s}^2$ of C3 for Mars and $-2\,\mathrm{km}^2/\mathrm{s}^2$ of C3 for the lunar mission. However, wide ranges of launch constraints should be additionally considered for more realistic mass budget estimation. $I_{\mathrm{sp\_m}}$ is assumed to be approximately 330 s, which is the same as the performance of the recent ExoMars onboard main engine [40]. In the following discussion, the "spacecraft mass" for the EMD and EMMGA cases directly refers to the mass of the Mars probe itself and the mass of the mothership, including the SmallSat's mass, respectively.

In Figure 2, the ratios of a spacecraft's estimated dry mass that can be delivered to Mars using the EMD and EMMGA transfer options are compared for each launcher. The spacecraft's dry mass ratio is calculated with the simple equation, $m_{\mathrm{dry}}^{\mathrm{EMMGA}}/m_{\mathrm{dry}}^{\mathrm{EMD}} \times 100$, where $m_{\mathrm{dry}}^{\mathrm{EMD}}$ and $m_{\mathrm{dry}}^{\mathrm{EMMGA}}$ are the spacecraft's dry mass that can be delivered to Mars using the EMD and EMMGA transfer options, respectively. The results indicate that a greater spacecraft dry mass can be delivered to Mars using the EMMGA transfer option if the ratio is greater than 100%, and the EMD option allows more mass to be carried to Mars if the ratio is less than 100%. Figure 2 reconfirms that the EMD transfer option can deliver a greater mass to Mars than the EMMGA case for most launch years, regardless of the launch vehicle used. However, for the year 2031, the given dry mass ratio is greater than 90% with the Proton M (95.24%) and Atlas V (92.09%) launch vehicles. This result indicates that the final mass delivery capability between the EMD and EMMGA transfer options can be minimized to less than 10% by selecting an appropriate launch date. Interestingly, the dry mass ratio for the year 2031 is greater than 100% with the Ariane 5 launcher (115.20%), which indicates that more mass (up to approximately 15% more) can be delivered to Mars when the EMMGA transfer option is used instead of the EMD transfer option. For example, if a Mars mission is planned for launch in 2031 for scientific purposes, then the proposed EMMGA transfer approach can be considered as an option. A dry mass ratio of 15% corresponds to approximately 200 kg, which is sufficient mass for a SmallSat to perform an additional mission around the Moon. Although not depicted in Figure 2, the dry mass ratio for the 2045 mission is also compared for the EMMGA and Type II-A of EMD options. As expected, the dry mass ratios are approximately 109.81% (Ariane 5), 90.78% (Proton M), and 87.78% (Atlas V) higher than those of the Type II-B case. For Ariane 5, a dry mass ratio of 9.81% corresponds to approximately 145 kg of additional mass. The suggested masses in the current subsection are all rough estimates and may be different if detailed launch constraints, such as mass penalties for injection inclinations and dependencies of C3 values on launch date changes, are considered. For example, an additional mass of 200 kg for a 2031 mission may lead to different results if mass penalties for injection inclinations are considered, although the assumed C3 value ($10\,\mathrm{km}^2/\mathrm{s}^2$) to derive the payload delivery capabilities is somewhat greater than the C3 value ($8.237\,\mathrm{km}^2/\mathrm{s}^2$, shown in Table 1) estimated for the 2031 mission. Details of the roughly estimated spacecraft dry mass budgets for each launch vehicle are compared in Table 4, and the values include the propellant masses.

Table 3: Typical payload delivery capabilities of the Ariane 5, Proton M, and Atlas V launch vehicles to target the Moon and Mars [35].

Launch vehicle	Target planet	
	Moon	Mars
Ariane 5	7,000 kg	4,500 kg
Proton M	5,890 kg	4,580 kg
Atlas V	6,740 kg	5,420 kg

4.2. SmallSat Mission Capabilities. Based on the launch opportunities of the previously analyzed EMMGA transfer option, this subsection further analyzes the capabilities of SmallSat missions. Indeed, the delta-V magnitude to deploy a SmallSat to be captured around the Moon, $\Delta\mathbf{V}_{\mathrm{MOI}}$, represents a major design factor when establishing the feasibilities of current conceptual missions. Therefore, the current analysis is performed based on the magnitude of SmallSat separation delta-Vs. To deploy a SmallSat into the orbit around the Moon, the delta-Vs generated from the SmallSat's separation mechanism and onboard propulsion system are required. However, this study ignores the magnitude of the delta-V generated from a SmallSat separation mechanism because the magnitude is small compared with the delta-V generated by the onboard propulsion system. As previously discussed, two different lunar capture scenarios, i.e., orbiting and impaction cases, are considered for the analysis. For the orbiting case, the SmallSat is ultimately assumed to be inserted into a circular orbit around the Moon with a 100-km altitude, and it has the same orbital inclination established during the hyperbolic approach of the mothership in the lunar SOI. In fact, a different range of inclinations is achievable during the lunar flyby, which can be accomplished by setting the inclination as the target constraint while formulating a trajectory optimization problem for more detailed analysis. However, the current analysis accepts this assumption to focus on the preliminary analysis. For an impacting case, the SmallSat is assumed to directly impact the lunar surface after being deployed from a certain altitude of the mothership's hyperbolic periapsis passage.

Among the several previously analyzed EMMGA launch opportunities, 2031 is selected as the year with the best mass budget performance. In Table 5, the associated delta-V

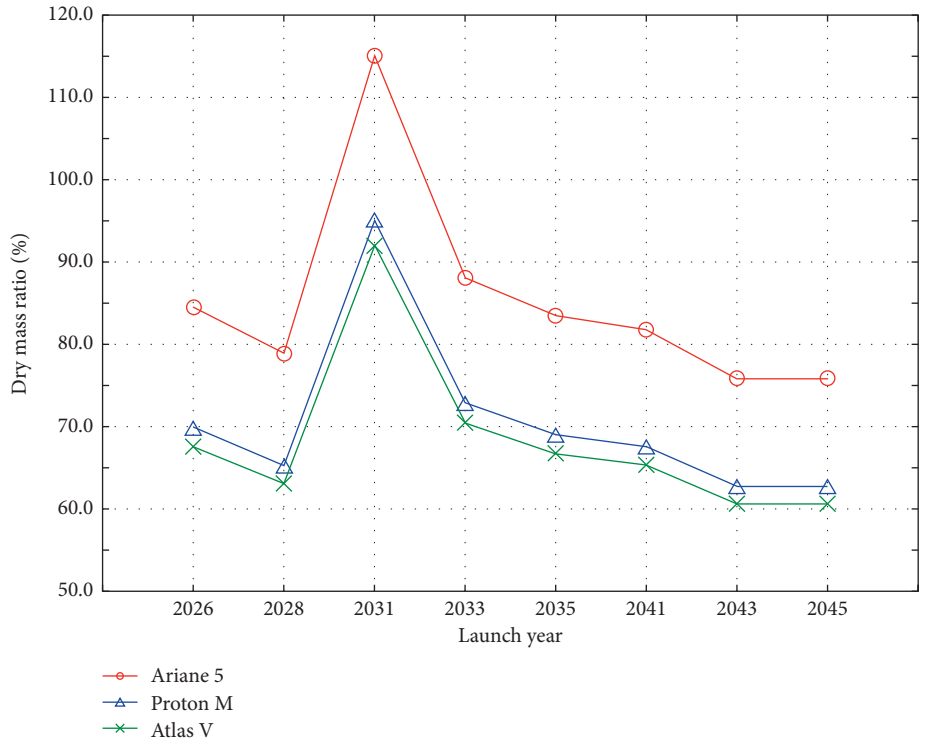

Figure 2: Annual variation history of the spacecraft dry mass ratio with respect to three different currently available heavy launch vehicles (Ariane 5, Proton M, and Atlas V).

Table 4: Details of the spacecraft's expected mass budgets for each mission year, which were derived from the payload capabilities of the following heavy launch vehicles: Ariane 5, Proton M, and Atlas V.

Launch vehicle	Launch year	EMD option		EMMGA option		Dry mass ratio (%)
		Prop. mass (kg)	Dry mass (kg)	Prop. mass (kg)	Dry mass (kg)	
Ariane 5	2026	2130.00	2370.00	4995.57	2004.43	84.58
	2028	2268.59	2231.41	5237.36	1762.64	78.99
	2031	3160.69	1339.31	5457.15	1542.85	115.20
	2033	2392.58	2107.42	5141.71	1858.29	88.18
	2035	2172.82	2327.18	5054.76	1945.24	83.59
	2041	2101.99	2398.01	5037.27	1962.73	81.85
	2043	2207.79	2292.21	5259.01	1740.99	75.95
	2045 (A type)	3030.16	1469.84	5385.95	1614.05	109.81
	2045 (B type)	2372.94	2127.06			75.88
Proton M	2026	2167.87	2412.13	4203.41	1686.59	69.92
	2028	2308.92	2271.08	4406.86	1483.14	65.31
	2031	3216.88	1363.12	4591.80	1298.20	95.24
	2033	2435.11	2144.89	4326.39	1563.61	72.90
	2035	2211.45	2368.55	4253.22	1636.78	69.10
	2041	2139.36	2440.64	4238.50	1651.50	67.67
	2043	2647.83	1932.17	4425.08	1464.92	75.82
	2045 (A type)	3084.03	1495.97	4531.90	1358.10	90.78
	2045 (B type)	2415.33	2164.67			62.74
Atlas V	2026	2565.47	2854.53	4810.02	1929.98	67.61
	2028	2732.39	2687.61	5042.83	1697.17	63.15
	2031	3806.88	1613.12	5254.45	1485.55	92.09
	2033	2881.72	2538.28	4950.74	1789.26	70.49
	2035	2617.04	2802.96	4867.01	1872.99	66.82
	2041	2531.74	2888.26	4850.17	1889.83	65.43
	2043	3133.50	2286.50	5063.68	1676.32	73.31
	2045 (A type)	3649.64	1770.36	5185.90	1554.10	87.78
	2045 (B type)	2858.08	2561.92			60.66

Table 5: SmallSat mission characteristics for the year 2031 for the orbiter and impactor mission case.

Periapsis altitude at deployment (km)	Periapsis velocity at deployment (km/s)	Delta-V for an orbiter mission (km/s)			Delta-V for an impactor mission (km/s)
		$\Delta \mathbf{V}_{rel}$	$\Delta \mathbf{V}_{sec}$	$\Delta \mathbf{V}_{MOI}$	$\Delta \mathbf{V}_{MOI}$
198.084	2.444	0.874	0.021	0.895	0.896

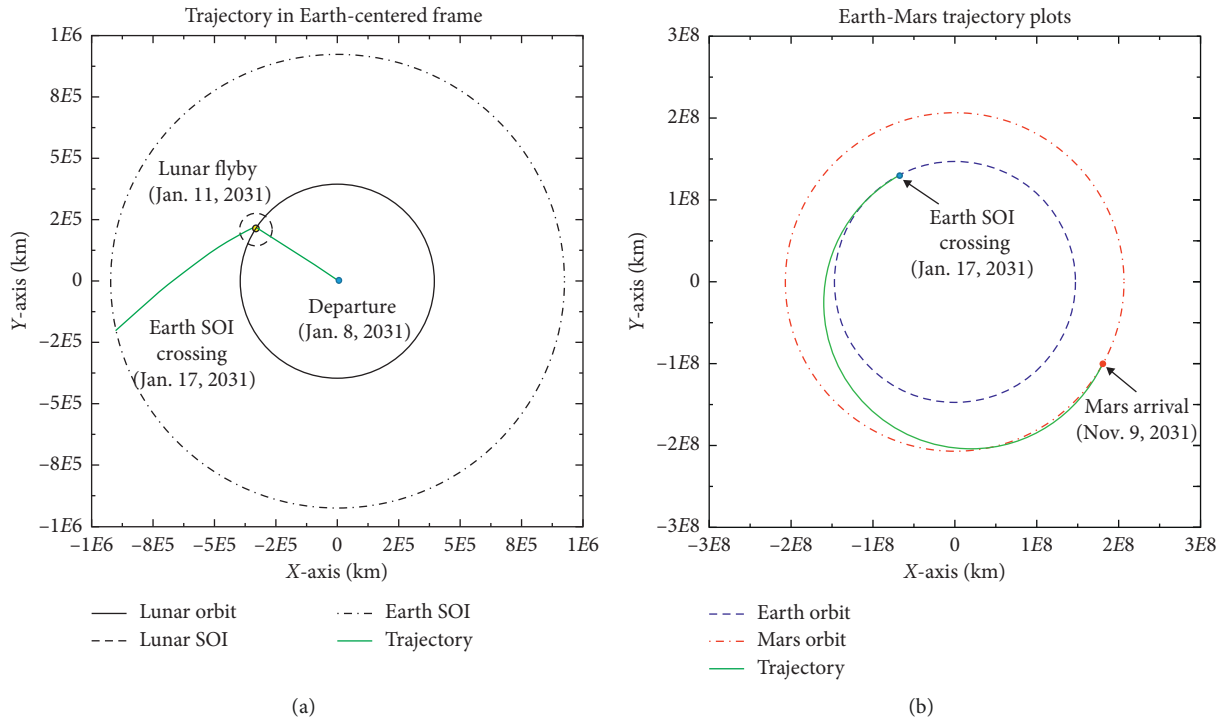

Figure 3: Example transfer trajectory of a 2031 mission. The left side shows the transfer trajectory inside of Earth's SOI, and the right side shows the Sun-centered Earth-Mars transfer trajectory.

characteristics for this year, including the periapsis altitude and velocity of the SmallSat at the moment of release, are shown. In the previous section, we showed that a total SmallSat mass of approximately 200 kg can be deployed around the Moon with an Ariane 5 launch vehicle using the EMMGA transfer option, which is comparable to that of the EMD transfer option. Assuming 277 s of I_{sp_s} [41], which is one of the highest I_{sp} values for currently available miniaturized thrusters, approximately 143.8 kg of dry mass is allowed when performing a mission around the Moon (143.876 kg for an orbiter and 143.823 kg for an impactor). Although the current analysis is performed using several assumptions that simplified the current problem, sending an approximately 200-kg-class SmallSat with a dry mass of approximately 140 kg with a single launch would certainly fulfill the requirements of the worldwide scientific community.

4.3. Example of a Transfer Trajectory. This subsection presents an example transfer trajectory of a 2031 mission that utilizes the EMMGA transfer option. Figure 3 depicts the entire transfer trajectory from Earth departure to Mars arrival. The left side of Figure 3 represents the trajectory of the 1st stage of the proposed conceptual mission in which the mothership departs the Earth on Jan. 8, 2031, performs a flyby of the Moon on Jan. 11, 2031, and escapes the Earth's SOI on Jan. 17, 2031. The total flight time of the mothership escaping the Earth's SOI is approximately 9.88 days. After the mothership escapes the Earth's SOI, it continues its journey to Mars (right side of Figure 3) and arrives on Nov. 9, 2031, which is approximately 296 days from its departure from Earth. The total TOF for the mothership is approximately 305 days, and the required $\Delta \mathbf{V}_{Total}$ is approximately 8.006 km/s. In Table 6, detailed trajectory information for the 2031 mission is summarized. As shown in Table 6, the values of t_{tof_E-M} and $\Delta \mathbf{V}_{Add.}$ are located at the lower limits of the search range under the current simulation conditions. Due to the simulation conditions discussed previously, the results of the 2031 case may not significantly differ for lower search range limits. However, the limits of these values can be further tuned for more detailed analysis by adapting an optimization scheme. During the mothership's lunar flyby, the SmallSat is released to perform its own mission. The SmallSat is deployed at an altitude of approximately 198.1 km at the periapsis passage of the mothership. The corresponding time is Jan. 11, 2031, 20 : 57 : 26.770 (TDB), and the SmallSat's mission around the Moon is then performed. Figure 4 shows an example of the SmallSat's mission

Table 6: Detailed trajectory data of the mothership for the 2031 mission.

t_{TLI} date	Jan. 8, 2031
t_{Arr} date	Nov. 9, 2031
t_{tof_E-M} (days)	4.000
ΔV_{add} (m/s)	−2.000
TLI maneuver direction	Ascending
t_p (TDB)	Jan. 11, 2031, 20 : 57 : 26.770
h_p (km)	198.084
t_{tof_SOI} (days)	9.885
t_{SOI} (TDB)	Jan. 17, 2031, 21 : 15 : 48.672
$\mathbf{v}_{SOI}$ (km/s)	1.187
ΔV_{Dep} (km/s)	3.112
ΔV_{SOI} (km/s)	2.004
ΔV_{Arr} (km/s)	2.890
ΔV_{Total} (km/s)	8.006
Total time of flight (days)	305.000

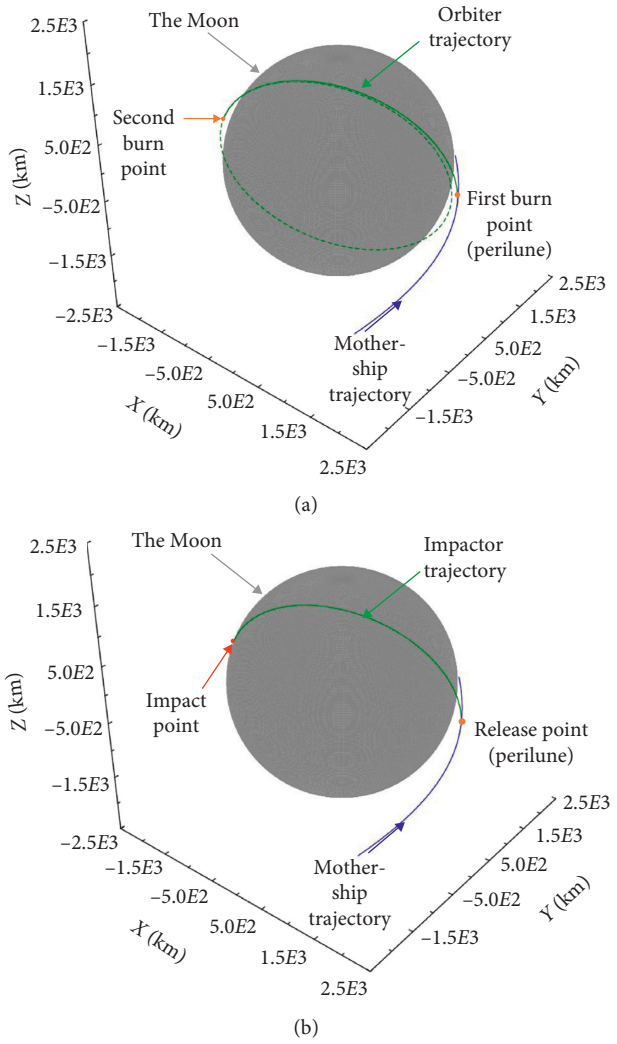

Figure 4: Example trajectory for a SmallSat mission around the Moon in 2031. The figure in the top shows the orbiter case, and the figure in the bottom is the impactor case.

trajectory around the Moon for the orbiter (top) and impactor cases (bottom). For the orbiter mission case, the SmallSat is inserted into a final 100-km-altitude circular orbit around the Moon after 61.2 min of transfer, and for the impactor case, approximately 58.8 min will be required to impact the lunar surface.

5. Conclusions

The current work proposes the concept of a multipurpose mission that can explore both the Moon and Mars with a single launch and analyzes potential launch opportunities for early-phase design work. For the mothership to reach Mars, the EMMGA trajectory is adapted for the trajectory design basis, and the daughtership is assumed to be released from the mothership during the lunar flyby to perform its own mission. To investigate potential launch opportunities, the associated delta-Vs have been derived and compared with the solutions provided by typical EMD transfer options with a simplified dynamic model to focus on the preliminary design studies. Additionally, two different lunar capture scenarios (orbiting and impacting cases) have been considered to investigate the SmallSat mission capabilities. The launch opportunities for the years 2026 through 2045 have been investigated. The analysis confirms that, regardless of transfer type and mission period, the EMMGA transfer options generally require a greater delta-V than the EMD options. However, two candidate launch years have been identified; the year 2031, and possibly 2045, may be the strongest candidate for a mission with the EMMGA option. In both years, the proposed conceptual mission is expected to be performed with only slightly greater delta-Vs, approximately 0.5 km/s and 0.6 km/s, respectively, than those of the Type II-A EMD transfer option of the 2031 and 2045 missions, respectively. To further improve the delta-V efficiency by adapting the strategies discussed, the overall mission delta-V difference between the EMD and EMMGA options are expected to be minimized compared to the current estimated values. The differences in delta-Vs are mainly caused by differences in the launch and arrival geometries, especially the geometry at the Mars arrival date, for the EMMGA and EMD transfer options. Three different currently available heavy launch vehicles (Ariane 5, Proton M, and Atlas V) were selected as candidate launchers, and the associated mass budgets were roughly analyzed. Interestingly, up to approximately 15% more dry mass can be delivered to Mars by using the EMMGA transfer option instead of the Type II-A EMD transfer option with the Ariane 5 launcher in the year 2031. For the 2045 mission, approximately 9% more dry mass can be delivered when the EMMGA and Type II-A of EMD options are compared for the Ariane 5 launcher. Although the estimation of the current launcher's payload delivery capabilities did not consider detailed launch constraints, rough dry mass ratio estimates of 15% and 9% correspond to approximately 200 kg and 145 kg, respectively, which appear to be sufficient for a SmallSat class mission around the Moon. Indeed, as the current work was performed under several assumptions to simplify the problem and focus on the preliminary analysis, many challenges still require resolution for this conceptual mission to be realized, and substantial research may be required. However, the narrowed candidate launch window

provided by the current work is a good starting point for more detailed optimal trajectory design and analysis to realize the proposed conceptual mission. Moreover, enabling a mission capable of reducing the overall mission costs while maximizing scientific merit will certainly be attractive to space scientists and supervisors who are willing to plan and propose such a mission.

Data Availability

The data used to support the findings of this study are available from the corresponding author upon request.

Conflicts of Interest

The authors declare that they have no conflicts of interest.

Acknowledgments

This work was supported by NRF-2014M1A3A3A02034761, NRF-2016M1A3A9913306, and the BK21 plus program through the National Research Foundation (NRF) funded by the Ministry of Education of Korea.

References

[1] J. Crusan, J. Bleacher, J. Caram et al., "NASA's gateway: an update on progress and plans for extending human presence to cislunar space," in *Proceedings of the IEEE Aerospace Conference*, Big Sky, MT, USA, March, 2019.

[2] T. D. Haws, J. S. Zimmerman, and M. E. Fuller, "SLS, the gateway, and a lunar outpost in the early 2030s," in *Proceedings of the IEEE Aerospace Conference*, Big Sky, MT, USA, March 2019.

[3] National Aeronautics and Space Administration (NASA), *NASA Taps 11 American Companies to Advance Human Lunar Landers*, National Aeronautics and Space Administration (NASA), Washington, DC, USA, 2019, https://www.nasa.gov/press-release/nasa-taps-11-american-companies-to-advance-human-lunar-landers.

[4] M. Xu and S. Xu, "Exploration of distant retrograde orbits around the moon," *Acta Astronautica*, vol. 65, no. 5-6, pp. 853–860, 2009.

[5] M. Xu and S. J. Xu, "Stability analysis and transiting trajectory design for retrograde orbits around moon," *Journal of Astronautics*, vol. 30, no. 5, pp. 1785–1791, 2009.

[6] M. Xu, Y. Wei, and S. Xu, "On the construction of low-energy cislunar and translunar transfers based on the libration points," *Astrophysics and Space Science*, vol. 348, no. 1, pp. 65–88, 2013.

[7] M. Xu, Y. Liang, and K. Ren, "Survey on advances in orbital dynamics and control for libration point orbits," *Progress in Aerospace Sciences*, vol. 82, pp. 24–35, 2016.

[8] Y. Liang, M. Xu, and S. Xu, "Low-energy weak stability boundary transfers to pluto's moons: preliminary trajectory design via triangular libration point," *Acta Astronautica*, vol. 156, pp. 219–233, 2019.

[9] G. Mengali, A. A. Quarta, C. Circi, and B. Dachwald, "Refined solar sail force model with mission application," *Journal of Guidance, Control, and Dynamics*, vol. 30, no. 2, pp. 512–520, 2007.

[10] A. A. Quarta and G. Mengali, "Semi-analytical method for the analysis of solar sail heliocentric orbit raising," *Journal of Guidance, Control, and Dynamics*, vol. 35, no. 1, pp. 330–335, 2012.

[11] L. Niccolai, A. A. Quarta, and G. Mengali, "Analytical solution of the optimal steering law for non-ideal solar sail," *Aerospace Science and Technology*, vol. 62, pp. 11–18, 2017.

[12] A. Caruso, A. A. Quarta, and G. Mengali, "Comparison between direct and indirect approach to solar sail circle-to-circle orbit raising optimization," *Astrodynamics*, vol. 3, pp. 1–12, 2019.

[13] S. Kemble, *Interplanetary Mission Analysis and Design*, Praxis Publishing, Chichester, UK, 2006.

[14] C. R. Cassell and P. A. Penzo, "LAMDA: a software tool for lunar-assist escape missions," in *Proceedings of the AAS/AIAA Astrodynamics Specialist Conference AAS 95-405*, Halifax, Nova Scotia, Canada, August 1995.

[15] A. V. Labunsky, O. V. Papkov, and K. G. Sukhanov, *Multiple Gravity Assist Interplanetary Trajectories*, Gordon and Breach Science Publishers, Amsterdam, The Netherlands, 1998.

[16] A. Poghosyan and A. Golkar, "CubeSat evolution: analyzing CubeSat capabilities for conducting science missions," *Progress in Aerospace Sciences*, vol. 88, pp. 59–83, 2017.

[17] R. L. Staehle, D. Blaney, H. Hemmati et al., "Interplanetary CubeSats: opening the solar system to a broad community at lower cost," *Journal of Small Satellites*, vol. 2, pp. 161–186, 2013.

[18] National Aeronautics and Space Administration (NASA), *Mars Cube One*, National Aeronautics and Space Administration (NASA), Washington, DC, USA, 2019, https://www.jpl.nasa.gov/cubesat/missions/marco.php.

[19] D. A. Williams, R. M. C. Lopes, J. Castillo-Rogez et al., "CubeSats to support future io exploration," in *Proceedings of the 49th Lunar and Planetary Science Conference 2018*, The Woodlands, TX, USA, March 2018.

[20] A. Shaw, R. Remblas, and P. Fulford, "Advantages of science cubesat and microsat deployment using DSG deep space exploration robotics," in *Proceedings of the Deep Space Gateway Science Workshop 2018*, Denver, CO, USA, February 2018.

[21] I. Garrick-Bethell, R. P. Lin, H. Sanchez et al., "Lunar magnetic field measurements with a CubeSat," in *Proceedings of the SPIE 8739, Sensors and Systems for Space Applications VI*, Baltimore, MD, USA, May 2013.

[22] Y.-J. Song, D. Lee, H. Jin, and B.-Y. Kim, "Potential trajectory design for a lunar CubeSat impactor deployed from a HEPO using only a small separation delta-V," *Advances in Space Research*, vol. 59, no. 2, pp. 619–630, 2017.

[23] R. W. Farquhar and D. W. Dunham, "Libration-point staging concepts for earth-mars transportation," in *Proceedings of the Manned Mars Mission Working Group Papers, a Workshop at Marshall Space Flight Center*, NASA/TM-89320, Huntsville, AL, USA, vol. 1, pp. 66-77, June 1985.

[24] M. Hanson John and A. W. Deaton, "Use of multiple lunar swingby for departure to mars," in *Proceedings of the AAS/AIAA Astrodynamics Conference AAS 91-499*, Durango, CO, USA, August 1991.

[25] J. Kawaguchi, H. Yamakawa, T. Uesugi, and H. Matsuo, "On making use of lunar and solar gravity assists in LUNAR-A, PLANET-B missions," *Acta Astronautica*, vol. 35, no. 9–11, pp. 633–642, 1995.

[26] S. Hernandez and B. W. Barbee, "Design of round-trip trajectories to near-earth Asteroids utilizing a lunar flyby," in *Proceedings of the 21st AAS/AIAA Space Flight Mechanics Meeting AAS 11-181*, New Orleans, LA, USA, February 2011.

[27] B. W. Barbee, T. Esposito, E. Piñon III et al., "A comprehensive ongoing survey of the near-earth asteroid population

for human mission accessibility," in *Proceedings of the AIAA Guidance, Navigation, and Control Conference AIAA 2010-8368*, Toronto, Ontario, Canada, August 2010.

[28] J. T. Betts, "Optimal lunar swingby trajectories," *The Journal of the Astronautical Sciences*, vol. 55, no. 3, pp. 349–371, 2007.

[29] D. A. Vallado, *Fundamentals of Astrodynamics and Applications*, Microcosm Press, Hawthorne, CA, USA, 4th edition, 2013.

[30] R. H. Battin, *An Introduction to the Mathematics and Methods of Astrodynamics*, AIAA, New York, NY, USA, 1987.

[31] R. V. Ramanan, "Integrated algorithm for lunar transfer trajectories using a pseudostate technique," *Journal of Guidance, Control, and Dynamics*, vol. 25, no. 5, pp. 946–952, 2002.

[32] E. M. Standish, "JPL planetary and lunar ephemerides, DE405/LE405," in *Jet Propulsion Laboratory Interoffice Memorandum*, Jet Propulsion Laboratory, La Cañada Flintridge, CA, USA, IOM 312.F-98-048, 1998.

[33] D. D. McCarthy and G. Petit, "IERS conventions (2003)," IERS Technical Note No. 32, 2004, https://www.iers.org/IERS/EN/Publications/TechnicalNotes/tn32.html?nn=94912.

[34] P. K. Seidelmann, B. A. Archinal, M. F. A'hearn et al., "Report of the IAU/IAG working group on cartographic coordinates and rotational elements: 2006," *Celestial Mechanics and Dynamical Astronomy*, vol. 98, no. 3, pp. 155–180, 2007.

[35] L.M. Burke, R. D. Falck, and M. L. McGuire, *Interplanetary Mission Design Handbook: Earth-To-Mars Mission Opportunities 2026 to 2045*, National Aeronautics and Space Administration, Washington, DC, USA, NASA/TM-2010-216764, 2010.

[36] P. J. Prince and J. R. Dormand, "High order embedded Runge-Kutta formulae," *Journal of Computational and Applied Mathematics*, vol. 7, no. 1, pp. 67–75, 1981.

[37] O. Montenbruck and E. Gill, *Satellite Orbits: Models, Methods and Applications*, Springer, Berlin, Germany, 2000.

[38] W. H. Press, S. A. Teukolsky, W. T. Vetterling, and B. P. Flannery, *Numerical Recipes in FORTRAN 77*, Cambridge University Press, Cambridge, UK, 2nd edition, 1992.

[39] R. Biesbroek, *Lunar and Interplanetary Trajectories*, Springer, Berlin, Germany, 2016.

[40] R. Lescouzères, M. Wolf, B. Wollenhaupt et al., "Propulsion system development and verification activities for the 2016 exomars trace gas orbiter," in *Proceedings of the Space Propulsion Conference 2014 SP2014_2968951*, Cologne, Germany, 2014.

[41] K. L. Zondervan, J. Fuller, D. Rowen et al., "CubeSat solid rocket motor propulsion systems providing delta-vs greater than 500 m/s," in *Proceedings of the AIAA/USU Conference of Small Satellites SSC14-X-1*, 2014.